Interfacing Thin-Wire and Circuit Subcell Models in Unstructured Time-Domain Field Solvers

Ian Jeffrey, *Member, IEEE*, and Joe LoVetri, *Member, IEEE*

***Abstract*—A method for driving and terminating Holland–Simpson based thin-wire models by arbitrary lumped-element circuits is proposed. The approach uses the fact that these thin-wire models result in modified Telegrapher's equations, and interfacing transmission lines and lumped-element circuits is straightforward. The thin-wire voltage and current at a circuit/wire junction can be written in terms of circuit nodal voltages and branch currents, permitting the circuit solution to act as a boundary condition for the thin-wire system. In this work, we provide the circuit/wire interfacing conditions and combine circuits with Edelvik's Holland–Simpson model that permits thin-wires to be arbitrarily oriented within an unstructured mesh. Edelvik's work, previously implemented for finite-difference and finite-element time-domain solvers is formulated for the finite-volume method. Numerical and experimental results for circuit-driven thin-wire antennas are provided to validate the method.**

***Index Terms*—Finite volume methods, lumped-circuit models, thin-wire models.**

I. Introduction

THIN-wire models are an important part of numerical methods for solving the time-domain Maxwell's equations in regions populated by thin-wire structures. Differentially formulated thin-wire models can be categorized into two distinct groups: First are thin-wire models that introduce an additional system of partial differential equations relating additional unknowns of current and charge-density (or an equivalent voltage) along the wire (we refer to these as *Holland–Simpson based models* [1]–[4]), and second are thin-wire models that do not introduce additional unknowns into the solution space. In these methods, current and voltage relations are enforced implicitly by constraining field components contributing to select contour integrals (we refer to this second class as *contour-integration based models* [5]–[8]). Both types of models appear to have made their debut within the framework of the finite-difference time-domain (FDTD) algorithm where the importance of subcell modeling is paramount. Attempting to resolve very small structural details such as thin wires within a standard FDTD framework is computationally prohibitive. In FDTD, where regularity of the computational grid is required, both types of thin-wire model are suitable. In fact, efficient implementations of the contour-integration models are dependent on the regularity of the FDTD grid.

Manuscript received May 24, 2011; revised September 08, 2011; accepted December 06, 2011. Date of publication January 31, 2012; date of current version April 06, 2012.

The authors are with the Department of Electrical and Computer Engineering, University of Manitoba, Winnipeg, MB, R3T 5V6, Canada (e-mail: ijeffrey@ee.umanitoba.ca; Joe_LoVetri@umanitoba.ca).

Digital Object Identifier 10.1109/TAP.2012.2186262

With increased computer resources and the proliferation of distributed and GPU-based computing, it has become practical to numerically solve the differential form of Maxwell's field equations using more flexible, yet more expensive algorithms. These include the finite-volume time-domain (FVTD), discontinuous-Galerkin time-domain (DGTD), and finite-element time-domain (FETD) methods. These algorithms are formulated on unstructured grids and, in principle, can resolve very small structural detail relative to the range of wavelengths in a broadband simulation. This is accomplished successfully for FVTD in [9]. Modeling small structures directly comes with a price: a localized increase in the mesh density and a decreased time step in explicit time-stepping schemes. Local time-stepping available in FVTD and DGTD formulations can help [9]. Still, these algorithms benefit from thin-wire models and improving thin-wire capabilities of these solvers is an area of ongoing research [2], [3], [10], [11].

In the class of unstructured time-domain solvers, existing thin-wire models are exclusively Holland–Simpson based. Within the context of unstructured grids, the Holland–Simpson models fall into two categories: mesh-dependent and mesh-independent models. In the former, thin-wire segments are made to conform to the volumetric grid. For example, a Holland–Simpson model for FVTD has been formulated in [12], requiring wire segments to be aligned with the edges of prismatic elements. Mesh-independent Holland–Simpson models allow the wire to be aligned arbitrarily in the volumetric grid. For example, Edelvik *et al.* have formulated mesh-independent Holland–Simpson models for FDTD and FETD [2], [10], [13]. The benefit of mesh-independent models is clear: A robust mesh-independent thin-wire model permits rapid iterative (re)placement of thin-wires without requiring the application engineer to regenerate the mesh.

In many applications, thin-wires are directly driven by circuits that are well characterized using lumped-element circuit models. A standard practice for driving and/or interconnecting contour-integration thin-wires models with subcell circuits is to modify the material parameters and/or fields local to the thin-wire [14], [15]. For example, a simple voltage source can be implemented by constraining the electric fields between its driving terminals. This is possible when the terminals are identified in, and associated with, the volumetric mesh. One of the source terminals can then also act as a termination point for a thin wire. A capacitor joining two thin wires can be modeled by assigning a permittivity to the volumetric cell(s) between the terminals of the connected wires [8]. These modifications are locally dependent on the structure of the grid and are permissible for contour-integration models because mesh-dependency is already required.

With the exceptions of the so-called "beam-voltage" sources used by Edelvik *et al.*, interfacing Holland–Simpson thin-wire models (structured or otherwise) with general lumped-element circuits is, to our knowledge, an open problem. The goal is to introduce lumped-element circuits that are independent of the mesh in order to retain the benefit of mesh-independent Holland–Simpson models.

The contributions of this work are twofold: First, it is well-known that the Holland–Simpson formulation results in a generalized form of the Telegrapher's transmission line equations. Interfacing circuits with transmission lines is a mature theory [16], [17] and so we develop the sufficient assumptions required to use this theory for coupling circuits to thin-wires. Second, we formulate the circuit-driven FVTD equivalent to Edelvik's thin-wire model using a one-dimensional, upwind, and flux-split FVTD formulation compatible with an FVTD field solver. Details of the temporal synchronization between the field model, thin-wire model, and circuit model are provided, and the resulting algorithm is validated numerically and experimentally. Sections II-A–II-B and Section III-A discuss the existing thin-wire model and a standard FVTD formulation and have been included for completeness. The contributing work, namely interfacing thin-wires and subcell circuits, adapting the thin-wire model to FVTD and the FVTD solution to the thin-wire equations are provided in Sections II-C–II-E and Sections III-B–III-E. Although implementation details are provided specifically for FVTD, the general concepts are given in sufficient detail that the method can be adapted to DGTD and FETD solvers.

II. A Circuit-Terminated Thin-Wire Model

In this section, we develop the general theory for terminating a mesh-independent thin-wire subcell model with arbitrary lumped-element circuits. The thin-wire model adopted is the Holland–Simpson based model of Edelvik *et al.* [2], [10]. Edelvik's approach extends the original Holland–Simpson model [1] by coupling the wire to the surrounding fields using a so-called *tube-distribution*. This approach appears to have been first introduced by Ledfelt [13], [18] and allows the wire to be arbitrarily oriented within the mesh. It has also been shown to preserve the stability of the underlying explicit field solver.

A. The Thin-Wire Equations

The Holland–Simpson thin-wire subcell model is formulated by assuming that the fields in the vicinity of each segment of wire correspond to those of an infinitely long wire embedded in a homogeneous and simple medium [1]. We suppose a wire of radius a [m], directed in the $\hat{\zeta}$ direction, around which we setup the cylindrical coordinates (ρ, ϕ, ζ), as shown in Fig. 1(a). The thin-wire carries a current $\mathcal{I}(t,\zeta)$ [A] and a per-unit-length (PUL) charge $\mathcal{Q}(t,\zeta)$ [C/m]. If the volumetric discretization is much finer than the smallest wavelength of interest, the fields near each segment of wire can be approximated by a static, ρ-directed, electric field and a static, ϕ-directed, magnetic field:

$$\mathcal{E}_\rho(t,\rho,\zeta) = \frac{\mathcal{Q}(t,\zeta)}{2\pi\epsilon\rho}, \quad \mathcal{H}_\phi(t,\rho,\zeta) = \frac{\mathcal{I}(t,\zeta)}{2\pi\rho} \tag{1}$$

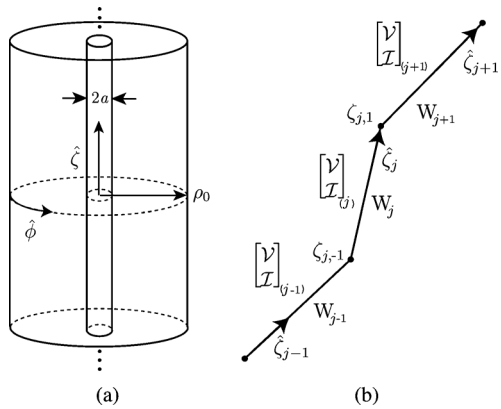

Fig. 1. (a) A portion of an infinite $\hat{\zeta}$-directed thin wire of radius a used to derive the thin-wire subcell model. Field/wire coupling occurs to the empirical distance ρ_0 where the medium is assumed homogeneous. (b) Discretization of the continuous wire domain into first-order wire segments.

where the dependence on ϕ is removed by the assumed symmetry and ϵ is the permittivity. We assume that the medium surrounding the wire has permittivity $\epsilon(\vec{r}) = \epsilon$, permeability $\mu(\vec{r}) = \mu$, and conductivity $\sigma(\vec{r}) = \sigma$ for locations $\vec{r}$ under consideration. The $\hat{\phi}$ component of Faraday's law

$$\frac{\partial \mathcal{E}_\zeta(t,\vec{r})}{\partial \rho} = \mu \frac{\partial}{\partial t}\mathcal{H}_\phi(t,\vec{r}) + \frac{\partial \mathcal{E}_\rho(t,\vec{r})}{\partial \zeta} \tag{2}$$

can be rewritten using the static field approximations (1) as

$$\frac{\partial \mathcal{E}_\zeta(t,\vec{r})}{\partial \rho} = \frac{\mu}{2\pi\rho}\left(\frac{\partial \mathcal{I}(t,\zeta)}{\partial t} + c^2 \frac{\partial \mathcal{Q}(t,\zeta)}{\partial \zeta}\right). \tag{3}$$

In (3), the velocity $c = (\epsilon\mu)^{-1/2}$ [m/s]. The ρ derivative is removed by integrating over any ρ branch transverse to the ζ direction, resulting in

$$\mathcal{E}_\zeta(t,\rho,\phi,\zeta) = \mathcal{I}(t,\zeta)R + \left(\frac{\partial \mathcal{I}(t,\zeta)}{\partial t} + c^2 \frac{\partial \mathcal{Q}(t,\zeta)}{\partial \zeta}\right)\frac{\mu}{2\pi}\ln\left(\frac{\rho}{a}\right) \tag{4}$$

where R [Ω/m] is a PUL resistance and where the term $I(t,\zeta)R$ accounts for the boundary condition at $\rho = a$.

Equation (4) relates the current and PUL charge on the thin wire to the longitudinal field component $\mathcal{E}_\zeta(t,\rho,\phi,\zeta)$ at some distance away from the wire. To remove the dependence on ρ, we adopt the distributional tube interpolation of Edelvik *et al.* and introduce a weighting function $g(\rho)$ [1/m^2] that couples the field, within a cylinder of finite radius ρ_0, to the wires in an average sense. The function $g(\rho)$ accounts for the finite thickness of the wire, i.e., $g(\rho) = 0 \; \forall \; \rho < a$ and has finite support, i.e., $g(\rho) = 0 \; \forall \; \rho > \rho_0$. Specific details of the coupling function are not required to develop the circuit/wire interface model. The coupling function $g(\rho)$ and distance ρ_0 are chosen as in [2], the latter being equal to 1.7 times the average edge length in the mesh. In the original reference, this distance has been selected empirically, and it is stated therein that if strongly inhomogeneous meshes are present, this distance should be taken as the average edge length in the vicinity of each wire segment [10].

Weighting both sides of (4) by $g(\rho)$ and integrating over a disk of radius ρ_0 transverse to the wire axis gives

$$\langle \mathcal{E}_\zeta(t,\zeta)\rangle = I(t,\zeta)R + L\left(\frac{\partial \mathcal{I}(t,\zeta)}{\partial t} + c^2\frac{\partial \mathcal{Q}(t,\zeta)}{\partial \zeta}\right) \quad (5)$$

where the average longitudinal electric field is given by

$$\langle \mathcal{E}_\zeta(t,\zeta)\rangle \triangleq \int_0^{2\pi}\int_0^{\rho_0} \mathcal{E}_\zeta(t,\rho,\phi,\zeta)g(\rho)\rho d\rho d\phi \quad (6)$$

and where the PUL inductance L [H/m], and its approximation used herein and in [2], is defined as

$$L \triangleq \frac{\mu}{2\pi}\int_0^{\rho_0} \ln\left(\frac{\rho}{a}\right) 2\pi g(\rho)\rho d\rho \approx \frac{\mu}{2\pi}\log\left(\frac{\rho_0 + a}{2a}\right). \quad (7)$$

Equation (5) provides a single equation relating the wire quantities $\mathcal{I}(t,\zeta)$ and $\mathcal{Q}(t,\zeta)$ to the average longitudinal field outside the wire. A second equation is obtained by conservation of charge along the wire axis:

$$\frac{\partial}{\partial \zeta} I(t,\zeta) + \frac{\sigma}{\epsilon}\mathcal{Q}(t,\zeta) = -\frac{\partial}{\partial t}\mathcal{Q}(t,\zeta). \quad (8)$$

Together, (5) and (8) form a system of two coupled partial differential equations for the wire quantities $\mathcal{I}(t,\zeta)$ and $\mathcal{Q}(t,\zeta)$. These are written in the space $\mathbb{R}^2$ (dropping the explicit spatial and temporal dependencies for notational brevity):

$$\frac{\partial}{\partial t}\begin{bmatrix}\mathcal{Q}\\ L\mathcal{I}\end{bmatrix} + \frac{\partial}{\partial \zeta}\begin{bmatrix}\mathcal{I}\\ Lc^2\mathcal{Q}\end{bmatrix} + \begin{bmatrix}\sigma\epsilon^{-1}\mathcal{Q}\\ R\mathcal{I}\end{bmatrix} = \begin{bmatrix}0\\ \langle \mathcal{E}_\zeta\rangle\end{bmatrix}. \quad (9)$$

B. The Thin-Wire Voltage

The thin-wire system of (9) is commonly written in terms of a voltage by defining a PUL capacitance C [F/m] satisfying $1/(LC) = \mu\epsilon = c^2$ [2], [10], [13]. This permits the definition of a wire voltage $\mathcal{V}(t,\zeta) = \mathcal{Q}(t,\zeta)/C$ [V] such that the system (9) can be rewritten as

$$\frac{\partial}{\partial t}\begin{bmatrix}C\mathcal{V}\\ L\mathcal{I}\end{bmatrix} + \frac{\partial}{\partial \zeta}\begin{bmatrix}\mathcal{I}\\ \mathcal{V}\end{bmatrix} + \begin{bmatrix}G\mathcal{V}\\ R\mathcal{I}\end{bmatrix} = \begin{bmatrix}0\\ \langle \mathcal{E}_\zeta\rangle\end{bmatrix} \quad (10)$$

where $G = \sigma C/\epsilon$ [S/m] is a PUL conductance. Clearly, this system of equations is in the form of modified Telegrapher's equations for a lossy transmission line. It is well established how to drive/terminate transmission lines using circuits by establishing a relationship between circuit voltages and currents to transmission line voltages and currents [16]. Interfacing the thin-wire model with circuit terminations should be straightforward, provided we understand how the voltage and current quantities on the thin wire are defined. Current is a physical quantity—its definition on a thin wire or a transmission line cannot be misconstrued. Voltage, on the other hand, is a relative quantity and must be defined carefully. Integrating the static electric field transverse to the wire from a to ρ for fixed ζ defines a voltage $\mathcal{V}^*(t,\rho,\zeta)$:

$$\mathcal{V}^*(t,\rho,\zeta) \triangleq \int_a^{\rho} \mathcal{E}_\rho(t,\rho',\zeta)d\rho' = \frac{\mathcal{Q}(t,\zeta)}{2\pi\epsilon}\ln\left(\frac{\rho}{a}\right). \quad (11)$$

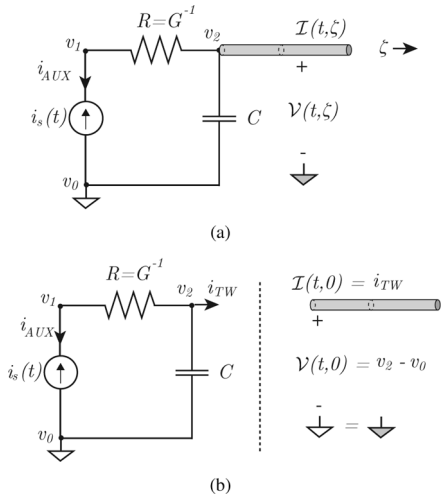

Fig. 2. (a) A wire/circuit interface. If the wire voltage at the interface is assumed to be the difference between two nodal voltages v_2 and v_0, the current and voltage at the interface results in two distinct problems (b): the circuit formulation with auxiliary current $i_{\rm TW}$ (left) and the thin-wire boundary condition (right).

Averaging $\mathcal{V}^*$ analogous to the computation of $\langle \mathcal{E}_\zeta(t,\zeta)\rangle$ such that

$$\begin{aligned}\langle \mathcal{V}^*(t,\rho,\zeta)\rangle &= \mathcal{Q}(t,\zeta)\frac{1}{2\pi\epsilon}\int_0^{\rho_0}\ln(\frac{\rho}{a})2\pi g(\rho)\rho d\rho\\ &= \mathcal{Q}(t,\zeta)Lc^2 = \frac{\mathcal{Q}}{C} = \mathcal{V}(t,\zeta)\end{aligned} \quad (12)$$

shows that the voltage $\mathcal{V}(t,\zeta) = \langle \mathcal{V}^*(t,\rho,\zeta)\rangle$ along the thin wire is a function of the coupling cylinder radius ρ_0 and represents the average voltage on the wire referenced to that distance.

C. Circuits as Thin-Wire Boundary Conditions

Consider a thin wire connected to a node in a circuit as shown in Fig. 2(a). On the thin wire, the system of partial differential (10) prevails. Its solution is unique, provided that initial conditions and boundary conditions are prescribed. Therefore, the solution of the circuit should establish a boundary condition at the wire/circuit interface. Before discussing this boundary condition, we must first select a circuit solution method and determine the relationships between circuit quantities and thin-wire quantities.

Motivated by the multiport-network, transmission-line formulation of LoVetri and Lapohos [16], we formulate the circuit using modified nodal analysis (MNA) and interface the circuit and thin-wires through auxiliary equations. MNA is a standard method for solving electric circuits consisting of $P+1$ nodal voltages v_p, including a reserved reference node $v_0 = 0$ [V] [19]. MNA seeks to determine the nodal voltages by enforcing Kirchoff's current law at each node using branch currents given in terms of nodal voltages. When a branch current cannot be written using nodal voltages, an *auxiliary current* and a corresponding *auxiliary equation* are required. This is the case, for example, for the current source in the circuit of Fig. 2(a).

Assuming that M auxiliary equations are required to solve a circuit with P nodes (excluding the reference node), we obtain the system of ordinary differential equations

$$\overline{\overline{G}} \cdot \underline{U}(t) + \overline{\overline{C}} \cdot \frac{d}{dt}\underline{U}(t) = \underline{S}(t) \tag{13}$$

where the constant square matrices $\overline{\overline{G}}$ and $\overline{\overline{C}}$ have dimension $(P+M)$. The $(P+M)$-length solution vector $\underline{U}$ consists of P unknown nodal voltages and M auxiliary currents while the source vector $\underline{S}$ accounts for forcing functions and initial conditions.

As shown in Fig. 2(b), the MNA system for the circuit can account for the thin wire by means of an auxiliary current i_{TW} if a relationship between circuit quantities and thin-wire quantities is established as follows.

1) The thin-wire voltage at a wire–circuit junction [and a function of ρ_0 according to (12)] can be represented (or approximated) by a difference between two nodal voltages in the circuit. This means relating the circuit reference (white triangle) of Fig. 2(a) to the thin-wire reference (gray triangle). Given this relationship, the wire can be connected to one of these two nodes, and the wire voltage at the interface can be converted to circuit nodal voltages, as shown in Fig. 2(b).
2) An auxiliary equation can be obtained from the relationship between the voltage and current on the thin wire to account for the unknown auxiliary current.
3) The solution of the circuit determines the nodal voltages and auxiliary currents. From these values, the boundary values for the wire at the junction are obtained.

Adhering to the above procedure gives a general method for interfacing an arbitrary number of thin-wire segments to an arbitrary circuit. In Section II-D, we will show that the assumption in item 1) always holds for certain circuits. In Section III-C, we develop the auxiliary equation required by item 2). Time synchronization between the thin wires and volumetric (14) and (15) are discussed in Section III-E.

Before proceeding, we note that the proposed circuit–wire interfacing does not impose any geometric constraints on the circuit beside its topological connection to the wires; the circuit can have arbitrary extent, provided that its solution still adheres to lumped-element circuit modeling assumptions. On the other hand, the formulation also permits a circuit to be introduced at a single point. This is the ideal case, where circuit quantities, such as nodal voltages, are truly spatially independent.

D. Compatibility of Thin-Wire and Circuit Voltages

Care must be taken when defining the voltage relationship between a circuit and a thin wire: the wire voltage should approximate the difference between two nodal voltages in the adjoining circuit. Three situations that do not require any approximations to make this connection are depicted in Fig. 3: First, some wire–circuit configurations do not require a circuit reference and can be consistently referenced to the wire. The balanced differentially driven wire configuration shown in Fig. 3 (top) serves as an example. Second, when a wire is connected to an open circuit as shown in Fig. 3 (bottom left), the current at the wire–circuit interface must be zero, and this can be used directly as the auxiliary equation independent of voltage reference. Last, when a wire is connected to a short-circuit, zero voltage is required at the circuit–wire interface, as shown in Fig. 3 (bottom right). From the definition of the thin wire (10), this condition is equivalent to enforcing $\partial \mathcal{I}(t,\zeta)/\partial\zeta = 0$ at the interface, independent of the voltage reference. The short-circuit and open-circuit conditions, are respectively equivalent to Edelvik's boundary conditions used when the wire is connected (normal to) a large PEC or to an open termination [2].

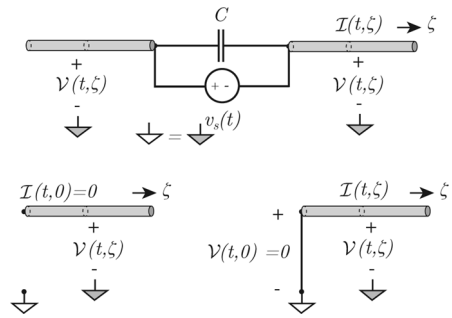

Fig. 3. The compatibility of the thin-wire voltage and circuit nodal voltages are independent of the coupling radius ρ_0 in at least three cases: differentially balanced circuits where the circuit is independent of the reference node (top); open circuits, where zero current is required at the interface independent of the voltage (bottom left); and short circuits where the voltage is zero at the interface independent of the current (bottom right).

E. Boundary Conditions for Hyperbolic Systems and the Thin-Wire Auxiliary Equation

The appropriate boundary conditions for the hyperbolic system (10) are best formulated in terms of the characteristic variables arising from the diagonalization of an equivalent lossless system [20]. A so-called characteristic variable flowing from a wire into a circuit is made up of a combination of the wire voltage and current and provides an auxiliary equation for the circuit. As upwind FVTD and DGTD algorithms are explicitly formulated using characteristic propagation, they are well suited to interface circuits as wire boundary conditions. An auxiliary equation compatible with the FVTD solution of the wire equations is given in Section III-C. In other numerical methods, such as FDTD and FETD, the discretization of the system (10) may associate an unknown current or voltage directly at the circuit–wire interface, making it necessary to enforce the circuit–wire boundary conditions in other ways.

III. The FVTD Formulation

What follows are the details for combining the circuit-driven thin-wire model with an FVTD field solver. The thin-wire equations are solved using a one-dimensional FVTD formulation for consistency with the three-dimensional solver.

A. Volumetric FVTD

To formulate the FVTD solution to the volumetric field problem, it is assumed that a finite computational domain V is partitioned into a set of N_V first-order polyhedral finite-volumes (or cells) $\{V_i\}$, with each V_i having an associated volume $|V_i|$ [m^3]. Each cell is bounded by K_i flat facets $S_{i,k}, k = 1, \ldots, K_i$. The material parameters associated with

the ith volume are constants: the permittivity in the ith cell is ϵ_i [F/m], the permeability is μ_i [H/m], and the conductivity is σ_i [S/m]. Maxwell's curl equations at time t and position $\vec{r}$ are integrated over each cell, and an application of the divergence theorem yields the system of equations in $\mathbb{R}^6$ for V_i,

$$\frac{d\vec{\boldsymbol{\mathcal{U}}}_{(i)}(t)}{dt} = \frac{-1}{|V_i|}\sum_{k=1}^{K_i}\iint_{S_{i,k}} \bar{\bar{\boldsymbol{\alpha}}}_i^{-1}\cdot\bar{\bar{\boldsymbol{A}}}_{i,k}\cdot\vec{\boldsymbol{\mathcal{U}}}(t,\vec{r})dS + \bar{\bar{\boldsymbol{\alpha}}}_i^{-1}\cdot\left(\bar{\bar{\boldsymbol{\sigma}}}_i\cdot\vec{\boldsymbol{\mathcal{U}}}_{(i)}(t)+\vec{\boldsymbol{\mathcal{S}}}_{(i)}(t)\right). \quad (14)$$

The solution vector $\vec{\boldsymbol{\mathcal{U}}}(t,\vec{r})$ contains both the electric field $\vec{\mathcal{E}}(t,\vec{r})$ [V/m] and the magnetic field $\vec{\mathcal{H}}(t,\vec{r})$ [A/m], i.e., $\vec{\boldsymbol{\mathcal{U}}}(t,\vec{r}) = [\vec{\mathcal{E}}(t,\vec{r})^T\ \vec{\mathcal{H}}(t,\vec{r})^T]^T$, where T denotes transposition. The source vector $\vec{\boldsymbol{\mathcal{S}}}(t,\vec{r}) = [-\vec{\mathcal{J}}(t,\vec{r})^T\ \vec{0}^T]^T$ supports impressed current densities $\vec{\mathcal{J}}(t,\vec{r})$ [A/m^2] under a total field formulation. Here and throughout, parenthesized subscripts denote the volumetric averages of the solution and source vectors over V_i. The constant physical medium associated with the ith cell is represented by the 6×6 diagonal matrices $\bar{\bar{\boldsymbol{\alpha}}}_i$ and $\bar{\bar{\boldsymbol{\sigma}}}_i$:

$$\bar{\bar{\boldsymbol{\alpha}}}_i = \mathrm{diag}(\epsilon_i,\ \epsilon_i,\ \epsilon_i,\ \mu_i,\ \mu_i,\ \mu_i)$$
$$\bar{\bar{\boldsymbol{\sigma}}}_i = \mathrm{diag}(-\sigma_i,-\sigma_i,-\sigma_i,0,0,0).$$

Finally, the 6×6 matrix $\bar{\bar{\boldsymbol{A}}}_{i,k}$ is a function of the outward normal to V_i on the surface $S_{i,k}$ as well as the physical medium in V_i [12].

FVTD discretizes the system (14) by associating the volumetric average $\vec{\boldsymbol{\mathcal{U}}}_{(i)}(t)$ with each volume V_i. The surface integrals are approximated by numerical quadrature. No surface values are stored, but are instead reconstructed to a desired level of accuracy from the volumetric averages of the surrounding cells. Our FVTD implementation uses a flux-split, upwind scheme where the fields are collocated in time. Details are available in [12], [21], and [22].

B. The FVTD Formulation of the Thin-Wire Equations

The one-dimensional system of thin wire (10) is hyperbolic and can be solved using a one-dimensional FVTD formulation. We assume the wire domain W is discretized into N_W first-order line segments W_j, each having length $|W_j|$, as shown in Fig. 1(b). The current and voltage on each wire segment are assumed to be related by a segment-dependent instance of the system (10). The physical parameters of the medium are assumed to be constants for a cylinder or radius ρ_0 surrounding each wire segment and are represented by ϵ_j, μ_j, and σ_j. The FVTD equations for segment j are obtained by averaging (10) over the segment and applying the one-dimensional divergence theorem. For W_j, this results in

$$\frac{d\boldsymbol{\mathcal{U}}_{(j)}(t)}{dt} = \frac{-1}{|W_j|}\sum_{k=-1}^{1} k\cdot\bar{\bar{a}}_j\cdot\boldsymbol{\mathcal{U}}(t,\zeta_{j,k}) - \bar{\bar{b}}_j\cdot\boldsymbol{\mathcal{U}}_{(j)}(t)+\bar{\bar{c}}_j\cdot\boldsymbol{\mathcal{S}}_{(j)}(t). \quad (15)$$

The thin-wire solution vector is $\boldsymbol{\mathcal{U}}(t,\zeta) = [\mathcal{V}(t,\zeta)\ \mathcal{I}(t,\zeta)]^T$ and the source vector is $\boldsymbol{\mathcal{S}}(t,\zeta) = [0\ \langle\mathcal{E}_\zeta(t,\zeta)\rangle]^T$. The matrices $\bar{\bar{a}}_j$, $\bar{\bar{b}}_j$ and $\bar{\bar{c}}_j \in \mathbb{R}^2\times\mathbb{R}^2$ are

$$\bar{\bar{a}}_j = \begin{bmatrix} 0 & \frac{1}{C_j}\\ \frac{1}{L_j} & 0\end{bmatrix}\quad \bar{\bar{b}}_j = \begin{bmatrix} \frac{G_j}{C_j} & 0\\ 0 & \frac{R_j}{L_j}\end{bmatrix}\quad \bar{\bar{c}}_j = \begin{bmatrix} \frac{1}{C_j} & 0\\ 0 & \frac{1}{L_j}\end{bmatrix} \quad (16)$$

where the parameters L_j, C_j, R_j, and G_j depend on the segment. The summation over k is a convenient way to represent the two ends of the wire located at $\zeta_{j,k}$, with k accounting for the outward normal and where $k=0$ does not contribute to the equation. The analogy between the one-dimensional system (15) and the volumetric system (14) is clear—the thin-wire equations are solved using the one-dimensional analog of the flux-split, upwind scheme used in the volumetric formulation. Flux-splitting results in a decomposition of the evaluation at each end of the segment into incoming (superscript $-$) and outgoing (superscript $+$) contributions at each end of the wire,

$$k\,\bar{\bar{a}}_j\cdot\boldsymbol{\mathcal{U}}(t,\zeta_{j,k}) = \bar{\bar{a}}^+_{j,k}\cdot\boldsymbol{\mathcal{U}}^+(t,\zeta_{j,k}) + \bar{\bar{a}}^-_{j,k}\cdot\boldsymbol{\mathcal{U}}^-(t,\zeta_{j,k}) \quad (17)$$

where $\boldsymbol{\mathcal{U}}^+$ is the value of the solution at $\zeta_{j,k}$ reconstructed from the inside of the segment and $\boldsymbol{\mathcal{U}}^-$ is reconstructed from outside the segment. Details can be found in [12] and [20].

C. The FVTD Thin-Wire Auxiliary Equation

While the flux-split approach to solving hyperbolic systems of equations like (14) and (15) are well documented [12], [20], [21], it is the flux-split details that provides the auxiliary equation used to interface thin-wires to circuits in an FVTD formulation. Diagonalizing the k-direction flux matrix $\bar{\bar{a}}_j(k) = k\,\bar{\bar{a}}_j$ by a similarity transformation gives

$$\bar{\bar{a}}_j(k) = k\,\bar{\bar{a}}_j = \bar{\bar{\psi}}_j(k)\cdot\bar{\bar{\lambda}}_j\cdot\bar{\bar{\psi}}_j^{-1}(k) \quad (18)$$

where the matrix of eigenvalues $\bar{\bar{\lambda}}_j = \mathrm{diag}(-c_j, c_j)$ and

$$\bar{\bar{\psi}}_j(k) = \begin{bmatrix} 1 & 1\\ -kY_j & kY_j\end{bmatrix}\quad \bar{\bar{\psi}}_j^{-1}(k) = \frac{1}{2}\begin{bmatrix} 1 & -kZ_j\\ 1 & kZ_j\end{bmatrix}. \quad (19)$$

Above, the segment velocity is c_j, the wire-segment impedance Z_j is defined as $Z_j \triangleq \sqrt{\mu_j/\epsilon_j} = \sqrt{L_j/C_j}$ and the wire-segment admittance $Y_j = Z_j^{-1}$.

The thin-wire characteristic variables $\mathcal{W}^{\pm}_{j,k}$, associated with the jth segment and direction k, are

$$\begin{bmatrix}\mathcal{W}^-_{j,k}(t,\zeta)\\ \mathcal{W}^+_{j,k}(t,\zeta)\end{bmatrix} = \bar{\bar{\psi}}_j^{-1}(k)\boldsymbol{\mathcal{U}}(t,\zeta) = \frac{1}{2}\begin{bmatrix}\mathcal{V}(t,\zeta)-kZ_j\mathcal{I}(t,\zeta)\\ \mathcal{V}(t,\zeta)+kZ_j\mathcal{I}(t,\zeta)\end{bmatrix} \quad (20)$$

and propagate unchanged along the wire segment in the direction of the segment outward normal k [20]. The characteristic leaving the segment at $\zeta_{j,k}$ is then $\mathcal{W}^+_{j,k}(t,\zeta_{j,k})$ and is directly related to the outgoing flux $\bar{\bar{a}}^+_{j,k}\cdot\boldsymbol{\mathcal{U}}^+(t,\zeta_{j,k})$ of (17).

Suppose now that segment j is connected to a circuit at $\zeta_{j,k}$. Using the method of Section II-C, the characteristic variable $\mathcal{W}^+_{j,k}$ can be written in terms of the auxiliary current and nodal voltages in the circuit. When $\mathcal{W}^+_{j,k}$ is known, this provides the required auxiliary equation for the circuit. For the example circuit of Fig. 2(b), the auxiliary equation present as the last row completes the MNA system

$$\begin{bmatrix} G & -G & 1 & 0 \\ -G & G - C\frac{d}{dt} & 0 & 1 \\ 0 & 0 & -1 & 0 \\ 0 & \frac{1}{2} & 0 & \frac{kZ_j}{2} \end{bmatrix} \begin{bmatrix} v_1 \\ v_2 \\ i_{AUX} \\ i_{\mathrm{TW}} \end{bmatrix} = \begin{bmatrix} 0 \\ 0 \\ i_s \\ \mathcal{W}^+_{j,k} \end{bmatrix} \quad (21)$$

where, for compactness, we have written the matrix as $\overline{\overline{G}} + d/dt\ \overline{\overline{C}}$. Note that, in this example, the solution to the circuit equation at time t provides the boundary voltage $\mathcal{V}(t, \zeta_{j,k}) = v_2(t)$ and the boundary current $\mathcal{I}(t, \zeta_{j,k}) = i_{\mathrm{TW}}(t)$. For general circuit–wire interfaces, the computed boundary values are used to provide the value for the incoming characteristic variable $\mathcal{W}^-_{j,k}$ at the interface. This value is directly related to the incoming flux $\overline{\overline{a}}^-_{j,k} \cdot \boldsymbol{\mathcal{U}}^-(t, \zeta_{j,k})$ required by (17).

D. Field-to-Wire and Wire-to-Field Coupling

In the Edelvik's tube-distribution model, coupling from the fields to the wires occurs in the thin wire (10) through the source term $\boldsymbol{\mathcal{S}}_{(j)}(t) = [0\ \langle \mathcal{E}_\zeta(t,\zeta)\rangle_{(j)}]^T$. For wire segment W_j, the source is computed as the $g(\rho)$-weighted, average ζ-directed field along the segment

$$\langle \mathcal{E}_\zeta(t,\zeta)\rangle_{(j)} = \frac{1}{|W_j|} \iiint_V \mathcal{E}_\zeta(t,\vec{r}) g(\rho_j) \Phi_j(\zeta) dV \quad (22)$$

where ρ_j is dependent on the orientation of segment W_j and where $\Phi_j(\zeta) = 1$ when $\zeta \in W_j$ and is zero otherwise [2]. The finite support of both $g(\rho_j)$ and $\Phi_j(\zeta)$ limit the integration over V to a set of cells $\{V_i^j\} \subset \{V_i\}$ in the vicinity of W_j. The integral over each cell in the set is performed numerically to the desired order of accuracy by reconstructing the electric field $\vec{\mathcal{E}}(t,\vec{r})$ from cell-averaged field values.

Coupling from the wire to the fields is performed as in [2], by defining a volumetric current density supported by the wires:

$$\vec{\mathcal{J}}(t,\vec{r}) = \sum_{j=1}^{N_W} I(t,\zeta) g(\rho_j) \Phi_j(\zeta) \hat{\zeta}_j. \quad (23)$$

The contribution from W_j is restricted to $\{V_i^j\}$. The source term $\vec{\boldsymbol{\mathcal{S}}}_{(i)}(t)$ required in the volumetric update of (14) for cell V_i, is computed by evaluating

$$\vec{\mathcal{J}}_{(i)}(t,\vec{r}) = \frac{1}{|V_i|} \iiint_{V_i} \sum_{j=1}^{N_W} I(t,\zeta) g(\rho_j) \Phi_j(\zeta) \hat{\zeta}_j dV. \quad (24)$$

Once again, the integral is computed using numerical quadrature to the desired order.

E. Temporal Synchronization of Circuits, Wires and Fields

We are now ready to deal with the issue of synchronizing the fields, wires and circuits. Without loss of generality, we will illustrate the procedure for a simple first-order explicit time step of length Δt in the loss-free case. Note that to ensure stability, we must select Δt as being the minimum of the time-step limit imposed by the volumetric FVTD update (14) and the wire FVTD update (15). When volumetric element dimensions are of the same linear size as wire segments, the three-dimensional time step will be required [20]. In practice, higher order temporal schemes are implemented using combinations of first-order steps. We begin by writing the field and wire equations in a general operator form as

$$\begin{aligned} \vec{\boldsymbol{\mathcal{U}}}^{n+1}_{(i)} &= \vec{\boldsymbol{\mathcal{U}}}^{n}_{(i)} - \Delta t \mathcal{L}_V(\vec{\boldsymbol{\mathcal{U}}}^n) - \Delta t \vec{\boldsymbol{\mathcal{S}}}^n_{(i)} \\ \boldsymbol{\mathcal{U}}^{n+1}_{(j)} &= \boldsymbol{\mathcal{U}}^{n}_{(j)} - \Delta t \mathcal{L}_W(\boldsymbol{\mathcal{U}}^n) - \Delta t \boldsymbol{\mathcal{S}}^n_{(j)} \end{aligned} \quad (25)$$

where the operators $\mathcal{L}_V$ and $\mathcal{L}_W$ account for the surface integrals over the cell boundaries for the field and wire equations, respectively, and n is the time-step index. When a thin wire is terminated at a circuit, the operator $\mathcal{L}_W$ requires knowledge of the circuit solution at time n, which is obtained from the circuit system (13) using a backward step

$$\underline{U}^n = \left(\overline{\overline{G}} + \frac{1}{\Delta t}\overline{\overline{C}}\right)^{-1} \left(\frac{1}{\Delta t}\overline{\overline{C}} \cdot \underline{U}^{n-1} + \underline{S}^n\right). \quad (26)$$

This circuit solution is dependent on the previous circuit solution and the circuit source vector $\underline{S}^n$, which includes any connected thin-wire characteristics variables at time n. Note that the implicit backward difference is essential: According to (13), a forward difference would require the computation of $\overline{\overline{C}}^{-1}$, which may not exist.

IV. Numerical and Experimental Results

For validating the circuit-driven thin-wire model, we consider the experimental setup shown in Fig. 4, consisting of an aluminum metal plate and two monopole antennas located at positions A and B. The monopole antennas are constructed to be 5 [cm] in length using SMA connectors and a 0.51-[mm]-diameter center conductor made from silver-covered copper-clad steel [23]. In all numerical simulations, circuits are introduced at a single point. All meshes were produced using Gmsh [24].

A. Single Monopole Over a PEC Ground Plane

As a first example, we consider a single monopole located at location A with the monopole at location B removed. In the numerical simulation, we consider a hemispherical domain as shown in Fig. 5. The radius of the computational domain is selected to be 0.1 [m]. The PEC surface (located in the x–y plane at $z = 0$) extends to the edge of the computational domain. The monopole is located at its center. While the PEC surfaces in the experimental and numerical simulations are not the same, we assume they are sufficiently large in both cases

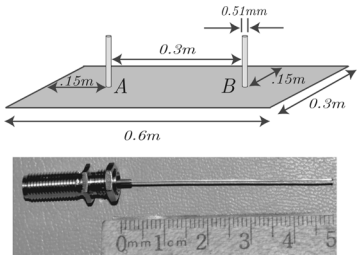

Fig. 4. Top: Experimental monopole configuration. Bottom: The 5-[cm]-long, 0.51-[mm]-diameter monopole.

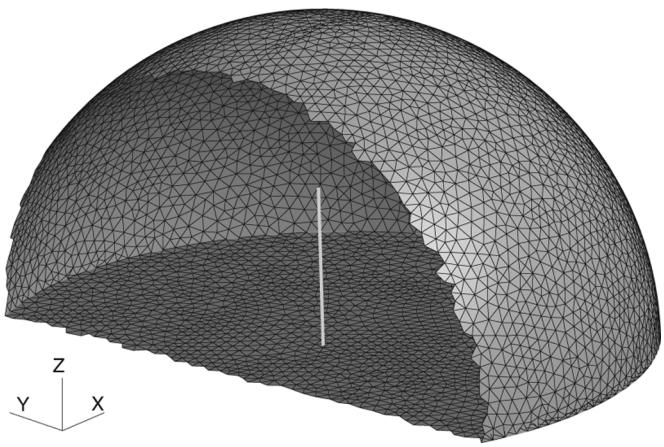

Fig. 5. Surface of the volumetric mesh used for the single monopole example.

to be approximately infinite. For all FVTD simulations, the absorbing boundary of the computational domain is enforced by a Silver–Müller boundary condition [21].

A discretization of the domain supporting frequencies up to 5 [GHz] at 10 samples per wavelength resulted in 600 000 tetrahedral elements. The wire was made up of 49 straight line segments and was driven and terminated using the circuit configuration shown in Fig. 6(a), where the voltage $\mathcal{V}_1(t)$ and the current $\mathcal{I}_1(t)$ were extracted from the simulation run. The voltage source $v_s(t)$ was set as the derivative of a Gaussian pulse having spectral content over the range 200 [MHz] to 5 [GHz]. The simulation was run for 15 000 time steps, or to roughly 5 [ns], and the monopole input impedance was computed as $Z_{in}(f) = \tilde{\mathcal{V}}_1(f)/\tilde{\mathcal{I}}_1(f)$, where $\tilde{\mathcal{V}}(f)$ denotes the Fourier transform of $\mathcal{V}(t)$. The input impedance was measured experimentally using a 9 [kHz]–8.5 [GHz] Agilent E5071C network analyzer. A comparison of the broadband numerical and experimental monopole results are shown in Fig. 7 and show good agreement. The small variations are consistent with other numerical simulations of resonant structures [1], [2], [10].

B. Dual Monopoles Over a PEC Ground Plane

As a second example, we consider the coupling between two monopoles corresponding to the experimental setup of Fig. 4. The mesh used for this problem is shown in Fig. 8. In this case, the numerical and experimental ground-planes correspond. The

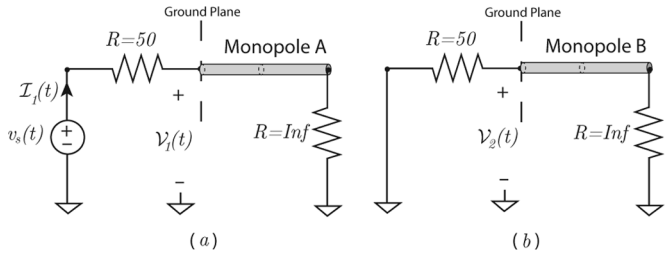

Fig. 6. Monopole driving circuits. (a) Monopole over PEC ground plane at location A. (b) Monopole over PEC ground plane at location B.

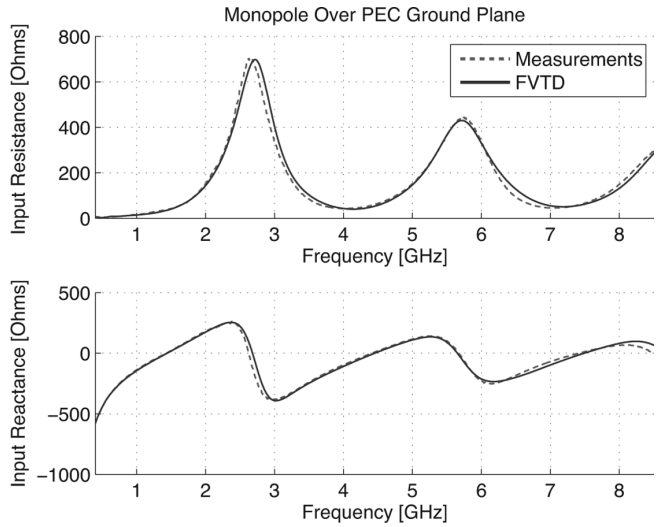

Fig. 7. Simulated and measured input resistance (top) and reactance (bottom) for a monopole over PEC ground plane.

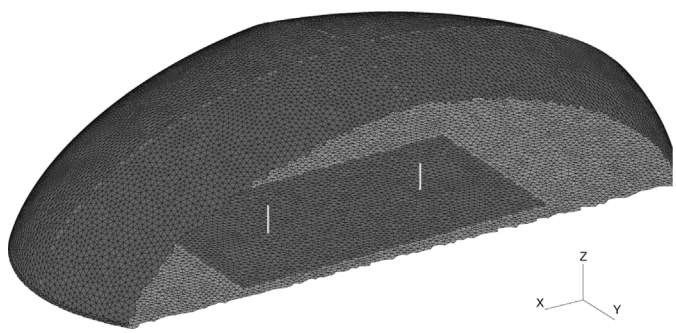

Fig. 8. Surface of the volumetric mesh used for the dual monopole example.

mesh contained roughly 2.3 million volumetric elements and each monopole consisted of 120 wire segments. The circuit configuration of Fig. 6 was used and $\mathcal{V}_1(t)$, $\mathcal{I}_1(t)$, and $\mathcal{V}_2(t)$ were extracted. The computed and measured S-parameters for the two-port network are shown in Figs. 9 and 10. A FEKO simulation [25] of the monopoles over an infinite ground plane is also shown.

C. Dipole Results

As a final example, we consider a dipole radiating in free space. Each dipole leg has dimensions equal to the monopoles of

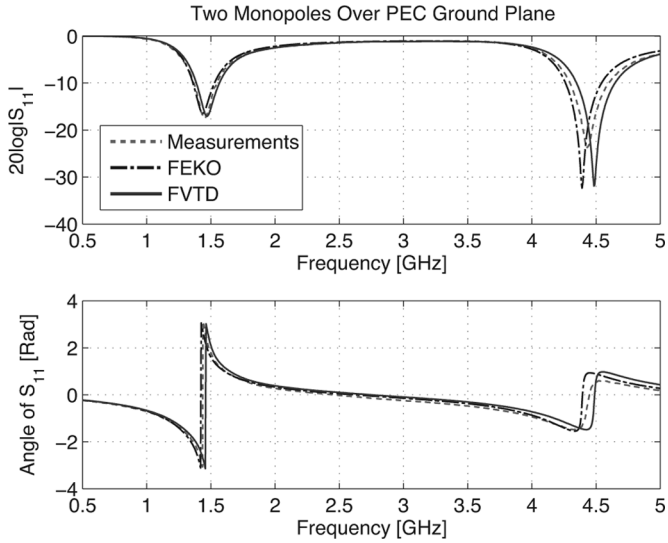

Fig. 9. S_{11} for two monopoles over a PEC ground plane, magnitude (top) and phase (bottom).

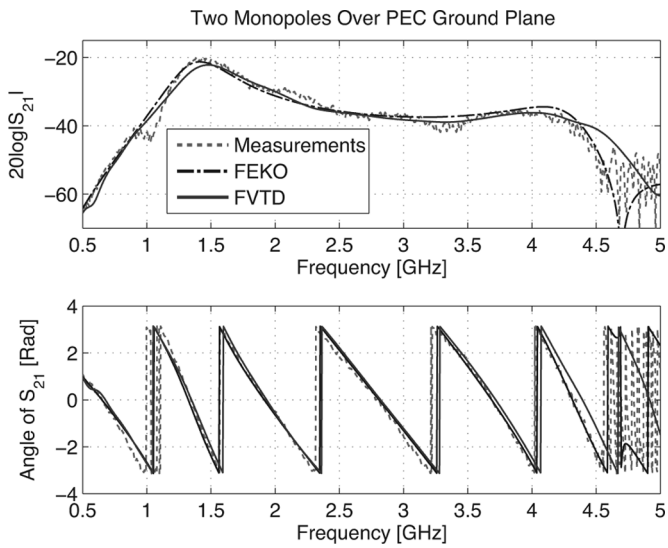

Fig. 10. S_{21} for two monopoles over a PEC ground plane, magnitude (top) and phase (bottom).

the previous examples, driven as shown in Fig. 11, where a capacitor is used to model feed capacitance. Without the capacitor, the input impedance should be exactly twice that of the single monopole example. A comparison of these results are shown in Fig. 12. Next, we introduce a 10 [pF] capacitor across the terminals of the dipole's driving circuit. The input impedance of this new configuration is equal to the input impedance without the capacitor in parallel with the impedance $Z_{cap}(f) = 1/(j2\pi fC)$ of the capacitor. In Fig. 13, we compare the input impedance when the capacitor is included as part of the FVTD simulation and when it is added to the unloaded input impedance of the dipole.

V. Conclusion

In this work, we have provided a method for interfacing arbitrary lumped-element circuits with Holland–Simpson type thin-wire models. Using modified nodal analysis and characteristic decomposition of the thin-wire solution allows circuits to be placed at a single point at wire terminals preserving the mesh-independent nature of the thin-wire model. The method has been implemented within an FVTD field solver and has been numerically and experimentally validated successfully.

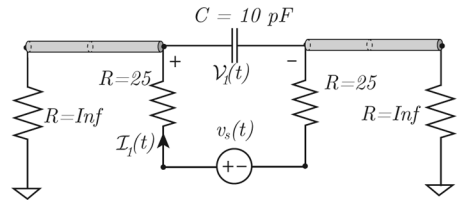

Fig. 11. Dipole driving circuit. In case 1, the capacitance is set to zero.

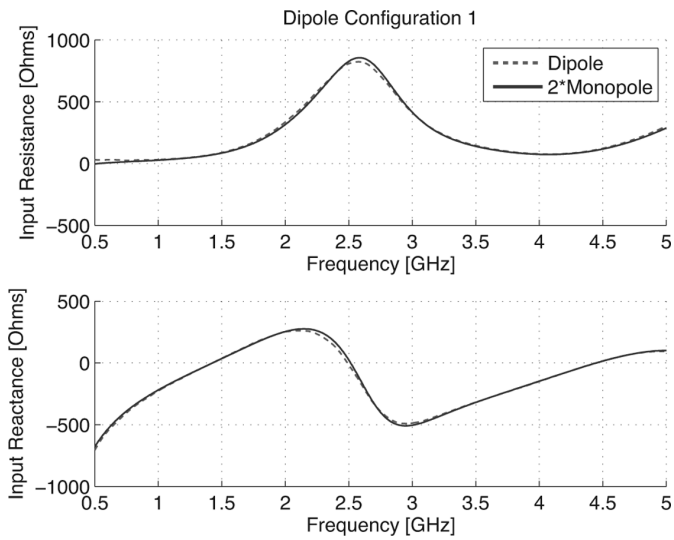

Fig. 12. Input resistance (top) and reactance (bottom) of the dipole compared to two times the monopole results.

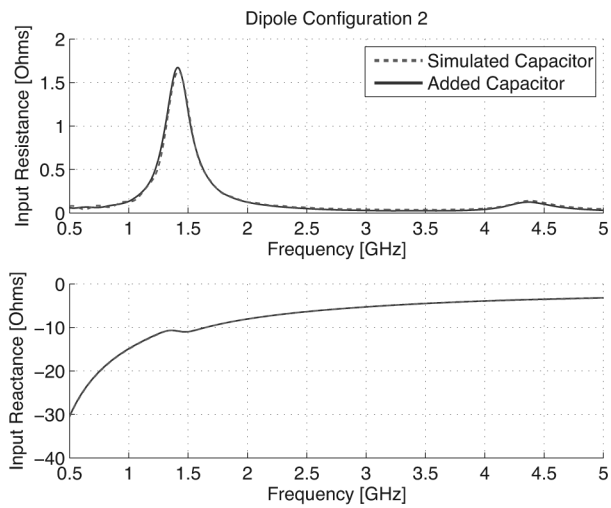

Fig. 13. Input resistance (top) and reactance (bottom) of the capacitively loaded dipole when the capacitor is included in the simulation and when its impedance is added after the fact.

REFERENCES

[1] R. Holland and L. Simpson, "Finite-difference analysis of EMP coupling to thin struts and wires," *IEEE Trans. Electromagn. Compatib.*, vol. EMC-23, no. 2, pp. 88–97, May 1981.

[2] F. Edelvik, "A new technique for accurate and stable modeling of arbitrarily oriented thin wires in the FDTD method," *IEEE Trans. Electromagn. Compatib.*, vol. 45, no. 2, pp. 416–423, May 2003.

[3] N. Gödel, T. Warburton, and M. Clemens, "Modeling effects of electromagnetic waves on thin wires with a high-order discontinuous Galerkin method," in *Spectral and High Order Methods for Partial Differential Equations*. Berlin, Germany: Springer, 2011, pp. 209–218.

[4] G. Zhang and C. Railton, "Treatment of arbitrarily-orientated multiwire bundles and terminated multiwire transmission lines in FDTD methods," *IET Microw., Antennas, Propag.*, vol. 1, no. 2, pp. 381–387, 2007.

[5] K. R. Umashankar, A. Taflove, and B. Becker, "Calculation and experimental verification of induced currents on coupled wires in an arbitrarily shaped cavity," *IEEE J. Antennas Propag.*, vol. 35, pp. 1248–1257, 1987.

[6] R. Makinen, J. Juntunen, and M. Kivikoski, "An improved thin-wire model for FDTD," *IEEE Trans. Microw. Theory Tech.*, vol. 50, no. 5, pp. 1245–1255, 2002.

[7] J. Nadobny, R. Pontalti, D. Sullivan, W. Wlodarczyk, A. Vaccari, P. Deuflhard, and P. Wust, "A thin-rod approximation for the improved modeling of bare and insulated cylindrical antennas using the FDTD method," *IEEE Trans. Antennas Propag.*, vol. 51, no. 8, pp. 1780–1796, 2003.

[8] D. Sullivan, P. Wust, and J. Nadobny, "Accurate FDTD simulation of RF coils for MRI using the thin-rod approximation," *IEEE Trans. Antennas Propag.*, vol. 58, no. 6, pp. 2004–2011, 2010.

[9] C. Fumeaux, D. Baumann, P. Leuchtmann, and R. Vahldieck, "A generalized local time-step scheme for efficient FVTD simulations in strongly inhomogeneous meshes," *IEEE Trans. Microw. Theory Tech.*, vol. 52, no. 3, pp. 1067–1076, Mar. 2004.

[10] F. Edelvik, G. Ledfelt, P. Lötstedt, and D. J. Riley, "An unconditionally stable subcell model for arbitrarily oriented thin wires in the FETD method," *IEEE Trans. Antennas Propag.*, vol. 51, no. 8, pp. 1797–1805, Aug. 2003.

[11] I. Jeffrey and J. LoVetri, "FVTD thin-wire models terminated by arbitrary lumped-element circuits," presented at the ACES Conf. 2010, Tampere, Finland, Apr. 2010.

[12] P. Bonnet, X. Ferrieres, B. Michielsen, P. Klotz, and J. Roumiguières, "Finite-volume time-domain method," in *Time Domain Electromagnetics*, S. M. Rao, Ed. New York: Academic, 1997, ch. 9, pp. 307–367.

[13] G. Ledfelt, "A stable subcell model for arbitrarily oriented thin wires for the FDTD method," *Int. J. Numer. Model.*, vol. 15, pp. 503–515, 2002.

[14] C. Railton, D. Paul, and S. Dumanli, "The treatment of thin wire and coaxial structures in lossless and lossy media in FDTD by the modification of assigned material parameters," *IEEE Trans. Electromagn. Compatib.*, vol. 48, no. 4, pp. 654–660, 2006.

[15] Y. Taniguchi, Y. Baba, N. Nagaoka, and A. Ametani, "An improved thin wire representation for FDTD computations," *IEEE Trans. Antennas Propag.*, vol. 56, no. 10, pp. 3248–3252, 2008.

[16] J. LoVetri and T. Lapohos, "Explicit upwind schemes for lossy MTL's with linear terminations," *IEEE Trans. Electromagn. Compatib.*, vol. 39, no. 3, pp. 189–200, Aug. 1997.

[17] A. Agrawal, H. Price, and S. Gurbaxani, "Transient response of multiconductor transmission lines excited by a nonuniform electromagnetic field," *IEEE Trans. Electromagn. Compatib.*, no. 2, pp. 119–129, 1980.

[18] G. Ledfelt, "Hybrid time-domain methods and wire models for computational electromagnetics," Ph.D. degree, Royal Inst. of Technol., Stockholm, Sweden, 2001.

[19] J. Vlach and K. Singhal, *Computer Methods for Circuit Analysis and Design*, 2nd ed. New York: Van Nostrand Reinhold, 1994.

[20] R. J. LeVeque, *Finite Volume Methods for Hyperbolic Problems*. Cambridge, U.K.: Cambridge Univ. Press, 2002.

[21] D. Firsov, J. LoVetri, I. Jeffrey, V. Okhmatovski, and C. G. W. Chamma, "High-order FVTD on unstructured grids using an object-oriented finite-volume time-domain computational engine," *ACES J.*, vol. 22, no. 1, pp. 71–82, Mar. 2007.

[22] D. Baumann, "A 3-D numerical field solver based on the finite-volume time-domain method," Ph.D. degree, Swiss Federal Inst. Technol., Zurich, Switzerland, 2006.

[23] A. Zakaria, C. Kaye, I. Jeffrey, and J. LoVetri, "Experimental validation of thin-wire FVTD models," presented at the ANTEM/URSI, Banff, AB, Canada, Feb. 2009.

[24] C. Geuzaine and J. Remacle, "GMSH: A 3-D finite element mesh generator with built-in pre-and post-processing facilities," *Int. J. Numer. Methods Eng.*, vol. 79, no. 11, pp. 1309–1331, 2009.

[25] Feko Comprehensive Electromagnetics Solutions, 2011 [Online]. Available: http://www.feko.info/

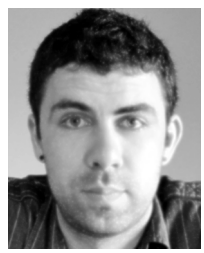

Ian Jeffrey (S'05–M'11) received the B.S. degree in computer engineering (Hons.), and the M.S. and Ph.D. degrees in electrical and computer engineering from the University of Manitoba, Winnipeg, MB, Canada in 2002, 2004 and 2011 respectively. In 2008, he was an Intern at Cadence Design Systems, Inc., Tempe, AZ, where he worked with the Department of Custom Integrated Circuits Advanced Research and Development. He currently holds a MITACS industrial postdoctoral fellowship with the National Research Council Canada's Institute for Biodiagnostics (NRC-IBD). His research interests include finite-volume and discontinuous galerkin time-domain methods, fast algorithms for computational electromagnetics, high-performance computing and inverse problems. He was a co-recipient of the 2007 ACES Outstanding Paper Award.

Joe LoVetri (S'84–M'84) received the B.Sc. (with distinction) and M.Sc. degrees, both in electrical engineering, from the University of Manitoba, Manitoba, Canada, in 1984 and 1987, respectively, and the Ph.D. degree in electrical engineering from the University of Ottawa, Ottawa, ON, Canada, in 1991. He also received an M.A. degree in philosophy from the University of Manitoba in 2006.

From 1984 to 1986, he was an EMI/EMC engineer at Sperry Defence Division, Winnipeg, Canada, and from 1986 to 1988, he held the position of TEMPEST Engineer at the Communications Security Establishment, Ottawa, Canada. From 1988 to 1991, he was a Research Officer at the Institute for Information Technology of the National Research Council of Canada. His academic career began in 1991 when he joined the Department of Electrical and Computer Engineering at The University of Western Ontario, where he remained until 1999. In 1997–1998, he spent a sabbatical year at the TNO Physics and Electronics Laboratory, The Netherlands, conducting research in time-domain computational methods and ground penetrating RADAR. In 1999, he joined the University of Manitoba, where he is currently a Professor in the Department of Electrical and Computer Engineering. From 2004 to 2009, he was the Associate Dean (Research and Graduate Programs) for the Faculty of Engineering. His main research interests lie in the areas of time-domain computational electromagnetics, modeling of electromagnetic compatibility problems, inverse problems, and biomedical imaging.

Dr. LoVetri received an URSI Young Scientist Award in 1993. He received the 2000 IEEE EMC Best Symposium Paper Award, and the 2007 ACES Outstanding Paper Award. In 2002, he received the University of Manitoba Rh Award for Outstanding Contributions to Scholarship and Research in the Applied Sciences. From 2005 to 2009, he was the National Representative for Commission E on the Canadian National Committee of URSI. In 2010, he co-chaired the Ultrawideband and Short-Pulse Electromagnetics Conference, which was part of AMEREM 2010 in Ottawa. He has been Chapter Chair for the IEEE EMC Ottawa Chapter as well as the Winnipeg Waves Chapter (AP/MTT). He has been a registered Professional Engineer in the province of Ontario, Canada, since 1994.